www.ietdl.org

Published in IET Renewable Power Generation
Received on 12th March 2009
Revised on 28th March 2010
doi: 10.1049/iet-rpg.2009.0021

ISSN 1752-1416

Integral variable structure direct torque control of doubly fed induction generator

S.Z. Chen[1] N.C. Cheung[2] K.C. Wong[2] J. Wu[3]

[1]Faculty of Automation, Guangdong University of Technology, Guangzhou 510006, People's Republic of China
[2]Department of Electrical Engineering, Hong Kong Polytechnic University, Kowloon, Hong Kong
[3]College of Electric Power, South China University of Technology, Guangzhou 510640, People's Republic of China
E-mail: eencheun@polyu.edu.hk

Abstract: This study proposes a novel integral variable structure direct torque control (IVS-DTC) scheme for a doubly fed induction generator (DFIG). The proposed scheme directly controls the torque and reactive power of the DFIG with rotor winding voltage, and hence no extra current control loops are required. Uncertainties in the parameters are included in the design procedure, which guarantees the robustness of the system. Compared to conventional direct torque control (DTC) scheme, the constant switching frequency in the proposed scheme does not introduce low-frequency sub-harmonics. Both computer simulation and hardware implementation results show that proposed scheme has satisfactory parametric robustness and generated power quality.

Nomenclature

u_{ds}, u_{qs}	direct and quadrature stator winding voltage
u_{dr}, u_{qr}	direct and quadrature rotor winding voltage
i_{ds}, i_{qs}	direct and quadrature stator winding current
i_{dr}, i_{qr}	direct and quadrature rotor winding current
λ_{ds}, λ_{qs}	direct and quadrature stator flux
λ_{dr}, λ_{qr}	direct and quadrature rotor flux
ω_e, ω_r, ω_s	stator, rotor and slip angular frequency
R_s, R_r	stator and rotor winding resistance
L_m	magnetising inductance
L_s, L_r	stator and rotor self-inductance
L_{ls}, L_{lr}	stator and rotor leakage inductance
p_n	number of pole pairs
T_e	electromagnetic torque of machine
Q_s	reactive power of stator
Δ	parameter deviation

Superscript

*	reference value

Subscripts

s, r	stator and rotor
d, q	synchronous d–q axis
α, β	stationary α–β axis
max, min	upper and lower limits of the parameter
0	nominal value of the parameter

1 Introduction

Owing to the increasing concern for environmental pollution and the gradual depletion of fossil energy resources, renewable energy and especially wind energy has attracted great interests in recent years. Grid-connected wind energy conversion system (WECS) can be divided into constant speed constant frequency (CSCF) type and variable-speed constant frequency (VSCF) type. Compared to CSCF-WECS, VSCF-WECS offers several advantages including maximising power capture, reducing mechanical stresses, improving power quality and providing frequency and voltage support to the power grid [1, 2].

VSCF-WECS can further be sub-divided into two categories: generators with full-power converters and the doubly fed induction generators (DFIG) with converters handling part of the generated power. The stator windings of DFIG are directly connected to the grid, and rotor windings are connected to the grid through a back-to-back PWM converter (Fig. 1). The rotor converter controls the voltage applied to the rotor winding of the DFIG. The grid converter controls the power flow between the DC-link and the grid to keep the DC-link capacitor voltage in a constant value. The main advantage of WECS based on DFIG is that the rating of the power converter is a portion of the generator rating [3].

The most popular and practical control scheme of DFIG is vector-oriented control based on proportional-integral (PI) controller [4, 5]. In the control scheme, the non-linear cross coupling is eliminated with feed-forward compensation, after which the motor model becomes linear and PI control techniques can be applied. However, since the decoupling procedure involves motor parameters, the resulting control scheme is sensitive to these parameters [6]. Furthermore, with the purpose of achieving expected closed-loop

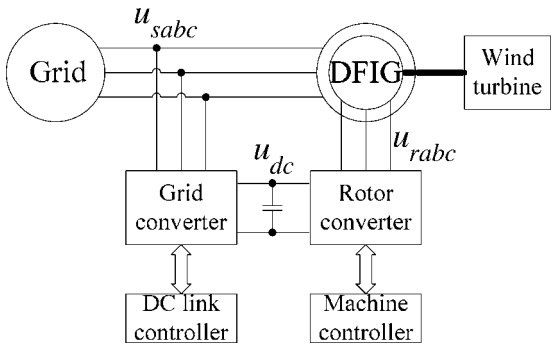

Fig. 1 *DFIG-based WECS*

dynamic response, the coefficients of PI controller should be designed according to motor parameters. Hence, the performance of vector control depends on the accuracy of motor parameters [7, 8].

In practice, motor parameters are generally obtained by identification experiments in which errors are unavoidable. The parameters will also be influenced by the environment and operating condition, for example, the resistance may vary with temperature and the inductance may vary with saturation.

Since the parameter depends on the vector control, a direct torque control (DTC) has been proposed [9, 10]. The DTC method directly controls the torque and flux of DFIG by selecting voltage vectors from a look-up table according to the logical output of the torque and flux hysteresis controllers. However, the hysteresis controls have some disadvantages, such as variable switching frequencies and current distortion, which will degrade the qualities of the output power [11, 12].

Based on the principle of DTC, hysteresis direct power control (DPC) is proposed in [7], in which the switching frequency is also not fixed. A constant frequency DPC is proposed in [8]. The required rotor voltage is calculated directly from the stator active and reactive power and their references, and hence the current controller is eliminated. It is well known that, in order to regulate the rotor rotating speed accurately, the total output active power of the DFIG, including stator power and rotor power, should be controlled. However, in [7, 8], only the stator active power is regulated but not the total power. Therefore the speed control accuracy, and hence the performance of maximum power point tracking of wind turbine, is degraded.

In recent years, a lot of research effort has been devoted to the application of variable structure control (VSC) techniques to the electrical drives and wind energy generation [6, 13–16]. Interest in this control approach has emerged because of its potential for being insensitive to variations of system parameters and external disturbances with a minimum of implementation complexity [6].

In order to solve the parametric robustness problem of vector control and power quality issue caused by variable switching frequency in DPC or DTC, this paper proposes an integral variable structure direct torque control (IVS-DTC) of a DFIG with a space vector modulation (SVM) scheme.

The paper is organised as follows. Section 2 gives the mathematical model of the DFIG. Section 3 simply describes the principle of IVSC. In Section 4, the IVS-DTC for decoupled control of DFIG is designed, and the parametric uncertainties are formally included. In Sections 5 and 6, simulation and hardware implementation results are reported to validate the satisfactory parametric robustness and generated power quality.

2 Model of DFIG

2.1 Mathematical model of DFIG

The equations describing the relationships among the electrical quantities of the DFIG in the stator-flux-oriented synchronous reference $d-q$ frame are

$$u_{ds} = R_s i_{ds} + \mathrm{d}\lambda_{ds}/\mathrm{d}t - \omega_e \lambda_{qs} \tag{1}$$

$$u_{qs} = R_s i_{qs} + \mathrm{d}\lambda_{qs}/\mathrm{d}t + \omega_e \lambda_{ds} \tag{2}$$

$$u_{dr} = R_r i_{dr} + \mathrm{d}\lambda_{dr}/\mathrm{d}t - (\omega_e - p_n\omega_r)\lambda_{qr} \tag{3}$$

$$u_{qr} = R_r i_{qr} + \mathrm{d}\lambda_{qr}/\mathrm{d}t + (\omega_e - p_n\omega_r)\lambda_{dr} \tag{4}$$

$$\lambda_{ds} = L_s i_{ds} + L_m i_{dr} = \lambda_s \tag{5}$$

$$\lambda_{qs} = L_s i_{qs} + L_m i_{qr} = 0 \tag{6}$$

$$\lambda_{dr} = L_r i_{dr} + L_m i_{ds} \tag{7}$$

$$\lambda_{qr} = L_r i_{qr} + L_m i_{qs} \tag{8}$$

$$T_e = -\frac{3}{2} p_n \frac{L_m}{L_s} \lambda_s i_{qr} \tag{9}$$

$$Q_s = \frac{3}{2}\frac{\omega_e \lambda_s}{L_s}(\lambda_s - L_m i_{dr}) \tag{10}$$

2.2 Direct relationship between electromagnetic torque/reactive power and rotor voltage

For the purpose to directly control the torque and reactive power, the direct relationship between the electromagnetic torque/stator reactive power and the rotor voltage will be developed. Substituting (5)–(8) into (3) and (4) and rearranging gives

$$\frac{\mathrm{d}i_{dr}}{\mathrm{d}t} = \frac{u_{dr}}{\sigma L_r} - \frac{R_r}{\sigma L_r} i_{dr} + \omega_s i_{qr} \tag{11}$$

$$\frac{\mathrm{d}i_{qr}}{\mathrm{d}t} = \frac{u_{qr}}{\sigma L_r} - \frac{R_r}{\sigma L_r} i_{qr} - \frac{\omega_s \lambda_s L_m}{\sigma L_r L_s} - \omega_s i_{dr} \tag{12}$$

where $\sigma L_r = (L_r - L_m^2/L_s)$ and $\omega_s = (\omega_e - p_n\omega_r)$.

Differentiating (9) and (10) with respect to time and substituting (12) and (11) into them yields

$$\frac{\mathrm{d}T_e}{\mathrm{d}t} = -\frac{3}{2} p_n \frac{L_m}{L_s} \lambda_s \left(\frac{u_{qr}}{\sigma L_r} - \frac{R_r}{\sigma L_r} i_{qr} - \frac{\omega_s \lambda_s L_m}{\sigma L_r L_s} - \omega_s i_{dr} \right) \tag{13}$$

$$\frac{\mathrm{d}Q_s}{\mathrm{d}t} = -\frac{3}{2} \omega_e \lambda_s \frac{L_m}{L_s} \left(\frac{u_{dr}}{\sigma L_r} - \frac{R_r}{\sigma L_r} i_{dr} + \omega_s i_{qr} \right) \tag{14}$$

2.3 Parametric uncertainty

The parameters of the DFIG are obtained by identification experiments in which errors are unavoidable, and furthermore, these parameters may vary with ambient temperature and exciting saturation. Considering the uncertainties of the machine parameters, it is assumed that

the parameters in (13) and (14) are bounded as follows

$$R_{\mathrm{r}\min} < R_{\mathrm{r}} = R_{\mathrm{r}0} + \Delta R_{\mathrm{r}} < R_{\mathrm{r}\max}$$

$$L_{\mathrm{m}\min} < L_{\mathrm{m}} = L_{\mathrm{m}0} + \Delta L_{\mathrm{m}} < L_{\mathrm{m}\max}$$

$$L_{\mathrm{s}\min} < L_{\mathrm{s}} = L_{\mathrm{s}0} + \Delta L_{\mathrm{s}} < L_{\mathrm{s}\max}$$

$$L_{\mathrm{r}\min} < L_{\mathrm{r}} = L_{\mathrm{r}0} + \Delta L_{\mathrm{r}} < L_{\mathrm{r}\max}$$

where $R_{\mathrm{r}0}$, $L_{\mathrm{m}0}$, $L_{\mathrm{s}0}$ and $L_{\mathrm{r}0}$ denote nominal values, and ΔR_{r}, ΔL_{m}, ΔL_{s} and ΔL_{r} denote deviations.

3 Integral variable structure control

The essential idea of traditional VSC algorithms is to enforce sliding mode in a predefined sliding surface of the system state space. Once the state of system reaches the sliding surface, the structure of the controller is adaptively changed to slide the state of system along the sliding surface. Hence, the system response depends only on the predefined sliding surface and remains insensitive to variations of system parameters and external disturbances. However, such insensitivity property is not guaranteed before sliding mode occurs, resulting in the loss of the robustness during the reaching phase. Furthermore, in order to reduce the chattering, the sign function of VSC is often replaced by saturation function in practical implementations, which will result in undesirable steady-state error.

To cope with the above problems, an integral action is introduced into traditional VSC, which forms the so-called integral variable structure control (IVSC). Sliding mode can be established in the initial time instant by properly choosing the initial condition of the integrator, and hence the reaching phase can be eliminated, implying that the invariance of the system to parametric uncertainty and external disturbances is guaranteed during the entire response. The integral action gives additional advantage of effectively minimising the steady-state error caused by the saturation function.

4 Design of proposed IVS-DTC scheme

The control objective is to independently control the electromagnetic torque and stator reactive power to track respective reference values, of which the control principles are similar. Hence, the torque controller and reactive power controller will be designed using the same procedure, and the deductive processes will be given at the same time.

The sliding surfaces of the proposed IVS-DTC for the electromagnetic torque and stator reactive power control of DFIG are given as follows

$$s_{T\mathrm{e}} = x_{T\mathrm{e}} + c\int_{-\infty}^{t} x_{T\mathrm{e}}(z)\mathrm{d}z_{T\mathrm{e}} = 0 \tag{15}$$

$$s_{Q\mathrm{s}} = x_{Q\mathrm{s}} + c\int_{-\infty}^{t} x_{Q\mathrm{s}}(z)\mathrm{d}z_{Q\mathrm{s}} = 0 \tag{16}$$

where c is the coefficient of the sliding surface, $z_{T\mathrm{e}}$, $z_{Q\mathrm{s}}$ are the dummy variables for the integration, state variables $x_{T\mathrm{e}}$, $x_{Q\mathrm{s}}$ are the errors between the real values and the reference values, and are defined as

$$x_{T\mathrm{e}} = T_{\mathrm{e}} - T_{\mathrm{e}}^{*} \tag{17}$$

$$x_{Q\mathrm{s}} = Q_{\mathrm{s}} - Q_{\mathrm{s}}^{*} \tag{18}$$

To guarantee the sliding mode in the initial time instant, the initial conditions of the integrators should be chosen as

$$I_{T\mathrm{e}0} = -x_{T\mathrm{e}0}/c, \quad I_{Q\mathrm{s}0} = -x_{Q\mathrm{s}0}/c$$

where $x_{T\mathrm{e}0}$ and $x_{Q\mathrm{s}0}$ are the initial conditions of $x_{T\mathrm{e}}$ and $x_{Q\mathrm{s}}$, $I_{T\mathrm{e}0}$ and $I_{Q\mathrm{s}0}$ are the initial conditions of the integrators defined as

$$I_{T\mathrm{e}0} = \int_{-\infty}^{0} x_{T\mathrm{e}}(z)\,\mathrm{d}z_{T\mathrm{e}}, \quad I_{Q\mathrm{s}0} = \int_{-\infty}^{0} x_{Q\mathrm{s}}(z)\,\mathrm{d}z_{Q\mathrm{s}}$$

Hence at $t = 0$

$$s_{T\mathrm{e}0}(t_0) = x_{T\mathrm{e}0} + cI_{T\mathrm{e}0} = 0 \tag{19}$$

$$s_{Q\mathrm{s}0}(t_0) = x_{Q\mathrm{s}0} + cI_{Q\mathrm{s}0} = 0 \tag{20}$$

Equations (19) and (20) mean that the system states are on the sliding surfaces in the initial time instant without the reaching phase, and the complete robustness can be obtained during the entire response.

The control inputs of the proposed scheme consists of the equivalent controls and switching controls, and are given as

$$u_{q\mathrm{r}} = u_{q\mathrm{r}}^{\mathrm{eq}} + \Delta u_{q\mathrm{r}} \tag{21}$$

$$u_{d\mathrm{r}} = u_{d\mathrm{r}}^{\mathrm{eq}} + \Delta u_{d\mathrm{r}} \tag{22}$$

The equivalent controls are used to control the nominal plant model, and the switching controls are added to ensure the desired performance despite parametric uncertainty.

By using the condition of the equivalent controls as $\dot{s} = 0$ [6], the equivalent controls are derived as

$$u_{q\mathrm{r}}^{\mathrm{eq}} = R_{\mathrm{r}0}i_{q\mathrm{r}} + \frac{\omega_{\mathrm{s}}\lambda_{\mathrm{s}}L_{\mathrm{m}0}}{L_{\mathrm{s}0}} + \sigma_0 L_{\mathrm{r}0}\omega_{\mathrm{s}}i_{d\mathrm{r}} - \frac{2}{3}\frac{\sigma_0 L_{\mathrm{r}0}L_{\mathrm{s}0}}{p_{\mathrm{n}}L_{\mathrm{m}0}\lambda_{\mathrm{s}}}\frac{\mathrm{d}T_{\mathrm{e}}^{*}}{\mathrm{d}t} + \frac{2}{3}\frac{\sigma_0 L_{\mathrm{r}0}L_{\mathrm{s}0}}{p_{\mathrm{n}}L_{\mathrm{m}0}\lambda_{\mathrm{s}}}cx_{T\mathrm{e}} \tag{23}$$

$$u_{d\mathrm{r}}^{\mathrm{eq}} = R_{\mathrm{r}0}i_{d\mathrm{r}} - \sigma_0 L_{\mathrm{r}0}\omega_{\mathrm{s}}i_{q\mathrm{r}} - \frac{2}{3}\frac{\sigma_0 L_{\mathrm{r}0}L_{\mathrm{s}0}}{\omega_{\mathrm{e}}\lambda_{\mathrm{s}}L_{\mathrm{m}0}}\frac{\mathrm{d}Q_{s}^{*}}{\mathrm{d}t} + \frac{2}{3}\frac{\sigma_0 L_{\mathrm{r}0}L_{\mathrm{s}0}}{\omega_{\mathrm{e}}\lambda_{\mathrm{s}}L_{\mathrm{m}0}}cx_{Q\mathrm{s}} \tag{24}$$

The switching controls are given as

$$\Delta u_{q\mathrm{r}} = K_{Te1}x_{T\mathrm{e}}\,\mathrm{sign}(s_{T\mathrm{e}}x_{T\mathrm{e}}) + K_{Te2}\,\mathrm{sign}(s_{T\mathrm{e}}) \tag{25}$$

$$\Delta u_{d\mathrm{r}} = K_{Qs1}x_{Q\mathrm{s}}\,\mathrm{sign}(s_{Q\mathrm{s}}x_{Q\mathrm{s}}) + K_{Qs2}\,\mathrm{sign}(s_{Q\mathrm{s}}) \tag{26}$$

The constants K in (25) and (26) are determined by the well-known sliding mode existence condition as

$$s_{T\mathrm{e}}\dot{s}_{T\mathrm{e}} < 0 \tag{27}$$

$$s_{Q\mathrm{s}}\dot{s}_{Q\mathrm{s}} < 0 \tag{28}$$

doi: 10.1049/iet-rpg.2009.0021

The constants to satisfy the inequality given in (27) are

$$K_{Te1} > \max\left|\frac{2}{3}\left(\frac{\sigma L_r L_s L_{m0} - \sigma_0 L_{r0} L_{s0} L_m}{L_m L_{m0}}\right)\frac{c}{p_n \lambda_s}\right| \quad (29)$$

$$K_{Te2} > \max\left|(R_r - R_{r0})i_{qr} + \left(\frac{L_m}{L_s} - \frac{L_{m0}}{L_{s0}}\right)\omega_s \lambda_s + (\sigma L_r - \sigma_0 L_{r0})\omega_s i_{dr} + \frac{2}{3}\left(\frac{\sigma_0 L_{r0} L_{s0} L_m - \sigma L_r L_s L_{m0}}{L_m L_{m0}}\right)\frac{1}{p_n \lambda_s}\frac{dT_e^*}{dt}\right| \quad (30)$$

The constants to satisfy the inequality given in (28) are

$$K_{Qs1} > \max\left|\frac{2}{3}\left(\frac{\sigma L_r L_s L_{m0} - \sigma_0 L_{r0} L_{s0} L_m}{L_m L_{m0}}\right)\frac{c}{\omega_e \lambda_s}\right| \quad (31)$$

$$K_{Qs2} > \max\left|(R_r - R_{r0})i_{dr} + (\sigma_0 L_{r0} - \sigma L_r)\omega_s i_{qr} + \frac{2}{3}\left(\frac{\sigma_0 L_{r0} L_{s0} L_m - \sigma L_r L_s L_{m0}}{\omega_e \lambda_s L_m L_{m0}}\right)\frac{dQ_s^*}{dt}\right| \quad (32)$$

In (30) and (32), dT_e^*/dt and dQ_s^*/dt will be infinite if the reference values are abruptly changed, and hence, K_{Te2} and K_{Qs2} cannot be determined if parametric uncertainty is considered. Therefore the rising and falling rates of input reference signals should be limited. Practically, in engineering implementations, rate limiters are also needed to avoid large stress on mechanical and/or electrical components.

The switching actions in (25) and (26) will cause chattering phenomenon, which can be conquered by introducing boundary layer. The sign functions are replaced by saturation functions in a small vicinity of the sliding surface, hence control discontinuities and switching action in the control loop is avoided. However, the boundary layer will cause steady-state errors. Fortunately, the integral action can deal with this problem. Fig. 2 shows the block diagram of the proposed IVS-DTC scheme. In Fig. 2, the stator flux, torque and reactive power are calculated in the stationary $\alpha-\beta$ frame as follows

$$\lambda_{\alpha\beta s} = \int (u_{\alpha\beta s} - R_s i_{\alpha\beta s})\,dt \quad (33)$$

$$T_e = 1.5 p_n(\lambda_{\alpha s} i_{\beta s} - \lambda_{\beta s} i_{\alpha s}) \quad (34)$$

$$Q_s = 1.5(u_{\beta s} i_{\alpha s} - u_{\alpha s} i_{\beta s}) \quad (35)$$

Since the stator voltages and currents in (33)–(35) are measured but not estimated, the stator flux, torque and reactive power can be accurately calculated without parameters of the generator, except for the stator resistance, whose impact on the system performance is negligible because of the relatively high grid frequency [7, 8]. As the flux estimation proposed in (33) will produce DC drift, in this implementation, the flux is estimated by subtracting the DC drift from (33). The DC drift is extracted from (33) with a low-pass filter with 40 Hz cut-off frequency.

5 Simulation results

The proposed IVS-DTC scheme is simulated in Matlab/Simulink. The nominal parameters of the DFIG are shown in the Appendix. The rising and falling rate of torque reference input is limited at ± 150 N m/s, and the rising and falling rate of stator reactive power reference input is limited at $\pm 10\,000$ VAR/s. The value of sliding surface

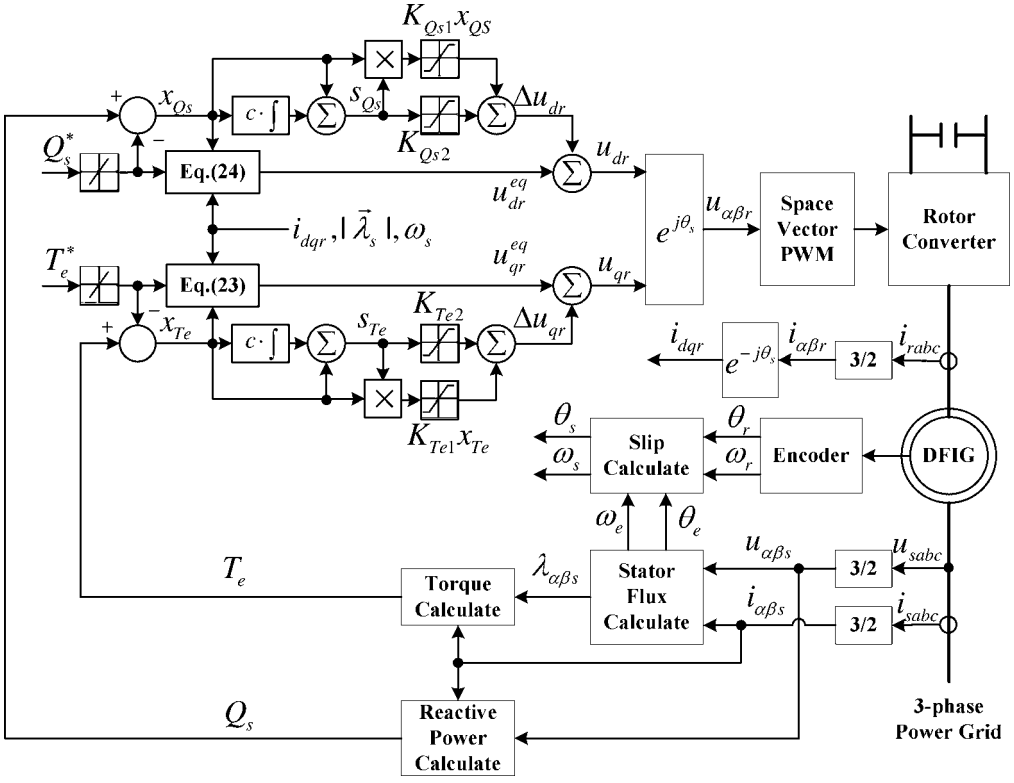

Fig. 2 *Block diagram of proposed IVS-DTC scheme*

coefficient c is chosen as 100. To determine the switching control, the maximum bounds of the parameter errors are assumed as $-0.5R_{r0} < \Delta R_r < 0.5R_{r0}$, $-0.5L_{m0} < \Delta L_m < 0.5L_{m0}$, $-0.5L_{r0} < \Delta L_r < 0.5L_{r0}$ and $-0.5L_{s0} < \Delta L_s < 0.5L_{s0}$. Under these assumptions and from (29) to (32), the constants in (25) and (26) can be chosen as $K_{Te1} = 0.76$, $K_{Te2} = 25.7$, $K_{Qs1} = 0.005$ and $K_{Qs2} = 20.5$.

In this simulation, the torque and reactive power reference values are manually input instead of being derived from the generator speed and the requirement of power grid so as to test the performance of proposed control scheme.

The responses to a step change of torque reference from 0 to -10 N m at 0.1 s are shown in Fig. 3. It shows that the torque of DFIG tracks the reference value quickly and the stator reactive power remains almost unchanged. Since the magnitude of the generator torque increases, the generator decelerates from super-synchronous speed to sub-synchronous speed, which does not influence the decouple control of the generator torque and reactive power.

The responses to a step change of reactive power reference from 1000 to 1500 VAR at a generator speed of 1440 RPM are shown in Fig. 4. The stator reactive power tracks the reference value quickly and the torque almost remains unchanged. The simulation results are very similar for other speeds within $\pm 20\%$ of the synchronous speed.

An existing cascaded PI vector control scheme proposed in [4] is also applied into the same DFIG system for comparison. The PI controllers of the inner rotor current loop and outer torque/reactive power loop are both designed to obtain first-order closed-loop responses, which time constants are 5 and 50 ms, respectively.

When the motor parameters are exact, the PI vector control scheme provides excellent control performance (solid line in Fig. 5). However, if the rotor resistance, rotor leakage inductance and stator leakage inductance of the DFIG are set to 75% of nominal value, the control performance degrades (dashed line in Fig. 5). The proposed IVS-DTC scheme is also simulated under the same conditions and the results are given in Fig. 6. Whether parametric errors exist or not, the response shows hardly any difference, which validate that the proposed scheme has better parametric robustness than PI vector control scheme.

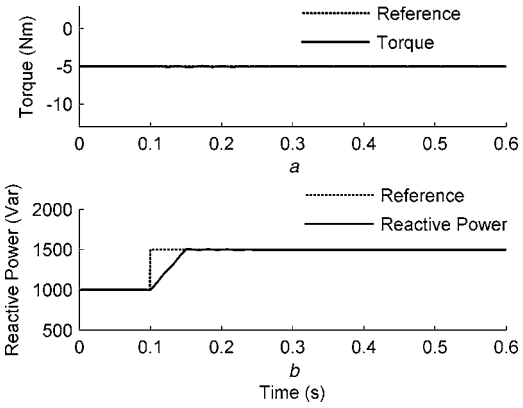

Fig. 4 *Simulation results under a step change in the reactive power reference*

a Torque
b Stator reactive power

6 Hardware experimental results

Fig. 7 shows the configuration of the experiment system. The rotor of the DFIG is mechanically coupled with a separately excited DC motor. The armature and field voltages of the DC motor can be manually adjusted to emulate a variable-speed prime mover with linear torque-speed characteristics. The rotor converter is an integrated power module (IPM)-based inverter, controlling the voltage applied to the rotor winding of the DFIG. The dSpace DS1103 is a prototyping card installed in a personal computer. It acquires stator voltages, stator currents, rotor currents and rotor position

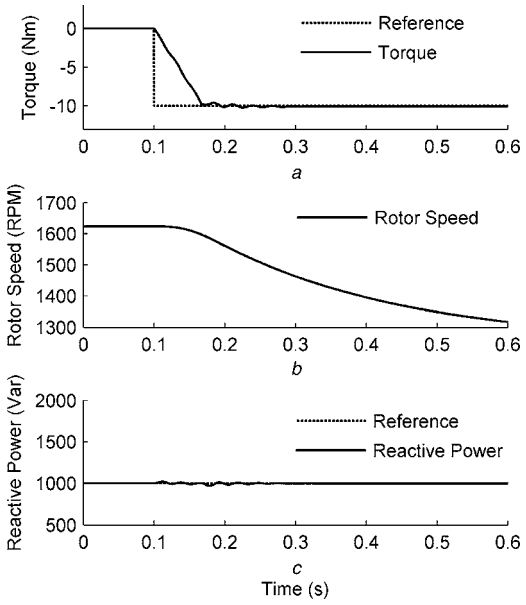

Fig. 3 *Simulation results under a step change in the torque reference*

a Torque
b Speed
c Stator reactive power

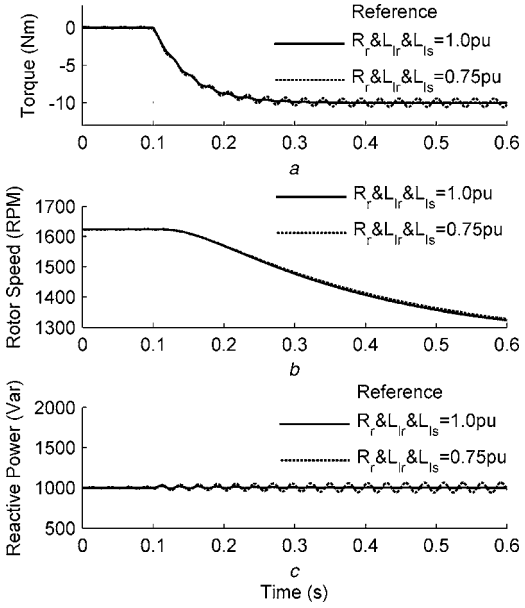

Fig. 5 *Simulation results with and without motor parametric errors under conventional PI vector control*

a Torque
b Speed
c Stator reactive power

doi: 10.1049/iet-rpg.2009.0021

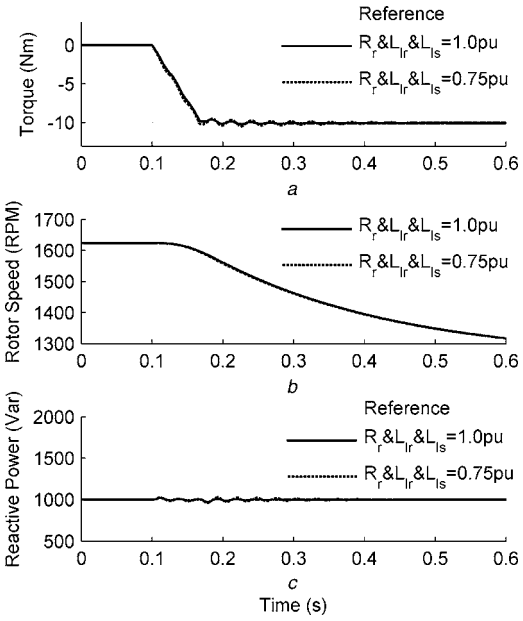

Fig. 6 *Simulation results with and without motor parametric errors under the proposed IVS-DTC scheme*

a Torque
b Speed
c Stator reactive power

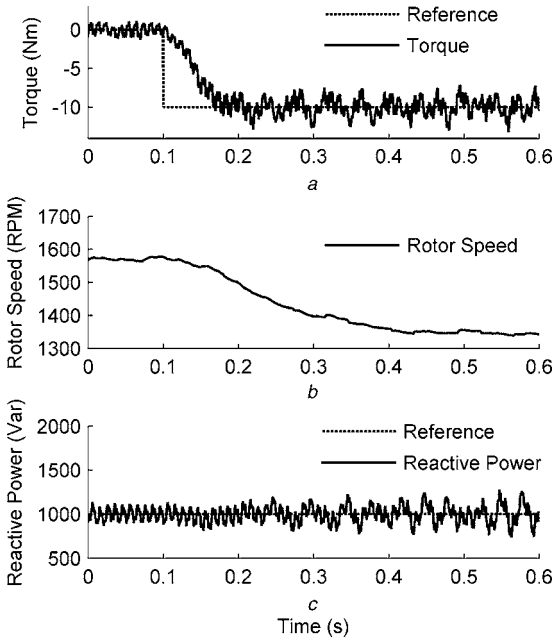

Fig. 8 *Experimental results under a step change in the torque reference*

a Torque
b Speed
c Stator reactive power

from the sensors and the encoder at a rate of 5 kHz, and processes them with the algorithm implemented with Matlab/Simulink. The card then generates 10 kHz SVPWM switching signal for the IPM control. The operating conditions and signals are displayed and stored in the personal computer in which the prototyping card is installed. The parameters of the DFIG are shown in the Appendix.

The responses to a step change of torque reference from 0 to 10 N m at 0.1 s are shown in Fig. 8. The torque follows the reference value quickly and the reactive power almost remains unchanged. Even the generator speed slows down from super-synchronous to sub-synchronous, the torque and the reactive power follow the reference values. The generator operates at the reference torque and reactive power steadily subsequent to the step change in the reference torque. The torque and reactive power ripples caused by unbalanced grid voltage, which will be discussed later, will not increase over time.

The responses to a step change of reactive power reference from 1000 to 1500 VAR at a generator speed of 1425 RPM are shown in Fig. 9. The stator reactive power follows the reference quickly and the torque almost remains unchanged.

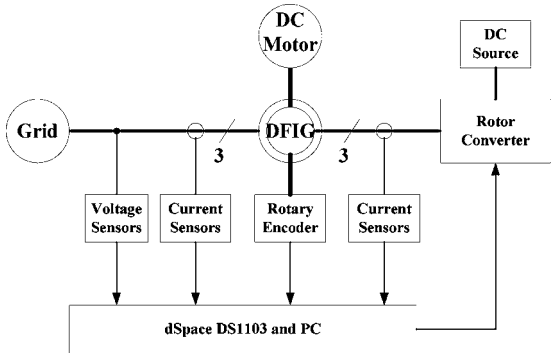

Fig. 7 *Configuration of experimental system*

Fig. 10 shows the harmonic spectra of stator and rotor current of the DFIG, which operates at −5 N m torque, 1000 VAR reactive power and 1425 RPM rotor speed. The dominant frequency of the stator current is 50 Hz, which equals to the grid frequency, and the dominant frequency of the rotor current is 2.5 Hz, which equals to the slip frequency. In Fig. 10, the proposed IVS-DTC scheme with constant switching frequency does not introduce low-frequency sub-harmonics, which are very common in conventional DTC schemes.

It is noticed that there are torque ripples and reactive power ripples in Figs. 8 and 9, whose dominant frequencies are 100 Hz. As suggested in [17–20], the ripples are caused by the unbalanced grid voltage. To estimate the degree of unbalance in the grid voltage, the measured grid voltage is

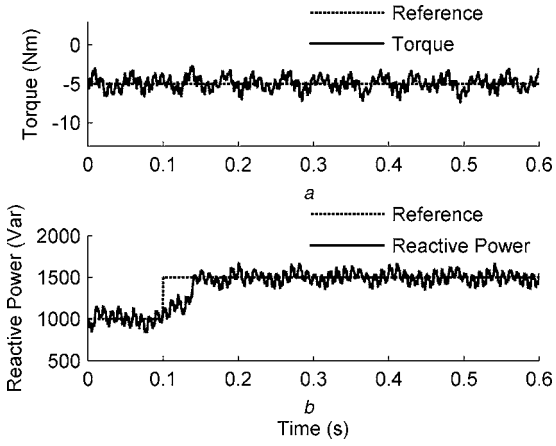

Fig. 9 *Experimental results under a step change in the reactive power reference*

a Torque
b Stator reactive power

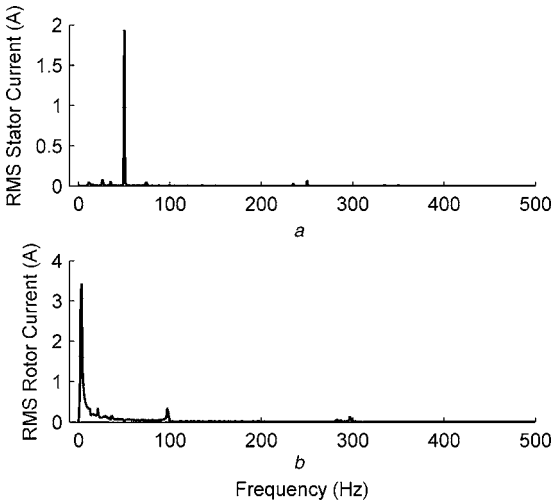

Fig. 10 *Harmonic spectra of stator and rotor current*

a Stator current
b Rotor current

decomposed into positive and negative sequence components using the decomposition algorithm based on signal delay cancellation proposed in [21]. The average positive sequence voltage is 308 V and the average negative sequence voltage is 3.29 V, hence the ratio of negative sequence to positive sequence voltage is 1.07%. Muljadi *et al.* [17] use the symmetrical component theory to analyse the effects of unbalanced voltages and finds that even a small stator voltage unbalance can cause large torque pulsation in an induction generator because of the low negative sequence impedance. The negative sequence component rotates at 50 Hz in the opposite direction of the positive sequence component, and causes a second harmonic (100 Hz) pulsation in the torque and reactive power [18]. Under unbalanced stator voltage, the rotor current of DFIG contains both the fundamental components of $f_e - p_n f_r$ and the harmonic components of $f_e + p_n f_r$ [19]. As shown in Fig. 10*b*, the fundamental component of rotor current is 2.5 Hz (50 − 47.5 Hz) and the harmonic component is 97.5 Hz (50 + 47.5 Hz). The existence of the harmonic components in the rotor verifies that unbalance component of the stator voltage causes the torque and reactive power ripples. Further investigation on advanced control schemes for DFIGs under unbalanced grid voltage will be performed.

7 Conclusions

This paper presents an IVS-DTC control scheme of the DFIG. Different from conventional variable switching frequency DTC scheme, the proposed IVS-DTC scheme employs a constant switching frequency, which does not introduce low-frequency sub-harmonics. Parametric uncertainties are formally included into the design procedure of the proposed scheme, and hence the robustness of the system can be guaranteed.

Simulation and hardware experimental results show that the proposed IVS-DTC scheme has satisfactory parametric robustness and generated power quality. The next research objective is to enhance the fault ride through capability of DFIG under unbalanced grid voltage, which is important for large-scale grid-connected wind turbines.

8 Acknowledgments

This work was supported by the National Natural Science Foundation of China under Grant 60534040, the National High Technology Research and Development of China under Project 863 Program 2007AA05Z244 and the Hong Kong Polytechnic University under Grant G-U497.

The authors gratefully acknowledge the contributions of K.F. Wong, W.W. Chan and C.K. Cheung on the experimental setup or their technical support/advices.

9 References

1 Ramtharan, G., Ekanayake, J.B., Jenkins, N.: 'Frequency support from doubly fed induction generator wind turbines', *IET Renew. Power Gener.*, 2007, **1**, (1), pp. 3–9
2 Hughes, F.M., Anaya-Lara, O., Jenkins, N., Strbac, G.: 'Control of DFIG-based wind generation for power network support', *IEEE Trans. Power Syst.*, 2005, **20**, (4), pp. 1958–1966
3 Li, H., Chen, Z.: 'Overview of different wind generator systems and their comparisons', *IET Renew. Power Gener.*, 2008, **2**, (2), pp. 123–138
4 Pena, R., Clare, J.C., Asher, G.M.: 'Doubly fed induction generator using back-to-back PWM converters and its application to variable-speed wind-energy generation', *IEE Proc. Electr. Power Appl.*, 1996, **143**, (3), pp. 231–241
5 Muller, S., Deicke, M., De Doncker, R.W.: 'Doubly fed induction generator systems for wind turbines', *IEEE Ind. Appl. Mag*, 2002, **17**, (1), pp. 26–33
6 Utkin, V.I., Güldner, J., Shi, J.X.: 'Sliding mode control in electromechanical systems' (CRC, Florida, 1999)
7 Xu, L., Cartwright, P.: 'Direct active and reactive power control of DFIG for wind energy generation', *IEEE Trans. Energy Convers.*, 2006, **21**, (3), pp. 750–758
8 Zhi, D., Xu, L.: 'Direct power control of DFIG with constant switching frequency and improved transient performance', *IEEE Trans. Energy Convers.*, 2007, **22**, (1), pp. 110–118
9 Arnalte, S., Burgos, J.C., Rodríguez-Amenedo, J.l: 'Direct torque control of a doubly fed induction generator for variable speed wind turbines', *Elect. Power Compon. Syst.*, 2002, **30**, (2), pp. 199–216
10 Yao, X., Jing, Y., Xing, Z.: 'Direct torque control of a doubly-fed wind generator based on grey-fuzzy logic'. Proc. Int. Conf. on Mechatronics and Automation, Harbin, China, August 2007, pp. 3587–3592
11 Buja, G.S., Kazmierkowski, M.P.: 'Direct torque control of PWM inverter-fed AC motors – a survey', *IEEE Trans. Ind. Electr.*, 2004, **51**, (4), pp. 744–757
12 Holtz, J.: 'Pulsewidth modulation for electronic power conversion', *IEEE Proc.*, 1994, **82**, (8), pp. 1194–1214
13 Chung, S.K., Lee, J.H., Park, J.W., Ko, J.S., Youn, M.J.: 'Current control of voltage-fed PWM inverter for AC machine drives using integral variable structure control'. Proc. Int. Conf. on Industrial Electronics, Control, and Instrumentation, Orlando, USA, November 1995, pp. 668–673
14 Drid, S., Tadjine, M., Nait-Said, M.S.: 'Robust backstepping vector control for the doubly fed induction motor', *IET Control Theory Appl.*, 2007, **1**, (4), pp. 861–868
15 Valenciaga, F., Puleston, P.F., Battaiotto, P.E.: 'Variable structure system control design method based on a differential geometric approach: application to a wind energy conversion subsystem', *IEE Proc. Control Theory Appl.*, 2004, **151**, (1), pp. 6–12
16 Xu, Z., Rahman, M.F.: 'Direct torque and flux regulation of an IPM synchronous motor drive using variable structure control approach', *IEEE Trans. Power Electron.*, 2007, **22**, (6), pp. 2487–2498
17 Muljadi, E., Yildirim, D., Batan, T.: 'Understanding the unbalanced-voltage problem in wind turbine generation'. Proc. Int. Conf. on Industry Application, Phoenix, USA, October 1999, pp. 1359–1365
18 Brekken, T., Mohan, N.: 'Control of a doubly fed induction wind generator under unbalanced grid voltage conditions', *IEEE Trans. Energy Convers.*, 2007, **22**, (1), pp. 129–135
19 Xu, L., Wang, Y.: 'Dynamic modeling and control of DFIG-based wind turbines under unbalanced network conditions', *IEEE Trans. Power Syst.*, 2007, **22**, (1), pp. 314–323
20 Wang, Y., Xu, L., Williams, B.W.: 'Compensation of network voltage unbalance using doubly fed induction generator-based wind farms', *IET Renew. Power Gener.*, 2009, **3**, (1), pp. 12–22
21 Zhou, Y., Bauer, P., Ferreira, J.A., Pierik, J.: 'Operation of grid-connected DFIG under unbalanced grid voltage condition', *IEEE Trans. Energy Convers.*, 2009, **24**, (1), pp. 240–246

doi: 10.1049/iet-rpg.2009.0021

10 Appendix

Machine parameters:
Stator-rated voltage: 380 V
Stator-rated current: 4.5 A
Rotor-rated voltage: 120 V
Rotor-rated current: 10 A
Operating frequency: 50 Hz
Synchronous speed: 1500 RPM
Magnetising inductance (referred to the stator): 0.2987 H
Rotor leakage inductance (referred to the stator): 0.0186 H
Stator leakage inductance: 0.0186 H
Rotor winding resistance (referred to the stator): 5.8985 Ω
Stator winding resistance: 2.6596 Ω
Stator-to-rotor turn ratio: 3.1667